ACS APPLIED MATERIALS & INTERFACES

Functional Nanostructured Materials (including low-D carbon)

Gold Nanoparticle Functionalized Cobalt-Nickel Phosphate 3D Nano-Ice Creams to Fabricate Stable and Sensitive Biosensor for Cytochrome c Assay

Caixia Wang, Mengsi Li, and Defang Liu

ACS Appl. Mater. Interfaces, **Just Accepted Manuscript** • DOI: 10.1021/acsami.0c10868 • Publication Date (Web): 08 Jul 2020

Just Accepted

is published by the American Chemical Society. 1155 Sixteenth Street N.W., Washington, DC 20036

Gold Nanoparticle Functionalized Cobalt-Nickel Phosphate 3D Nano-Ice Creams to Fabricate Stable and Sensitive Biosensor for Cytochrome c Assay

Caixia Wang [a], Mengsi Li [a] Defang Liu [a,b,*]

[a] *College of Chemistry and Chemical Engineering, Southwest University, Chongqing, 400715, China*

[b] *Key Laboratory of Biorheological Science and Technology, Ministry of Education, College of Bioengineering, Chongqing University, No.174, Shapingba Main Street, Chongqing 400030, China*

Abstract

Designing stable and sensitive luminol-based electrochemiluminescence (ECL) analytical platform in the neutral condition has attracted a lot of attention. Here, gold nanoparticle functionalized cobalt-nickel phosphate three-dimensional nano-ice creams (Au@$Co_3Ni_3(PO_4)_4$ NICs) are successfully prepared via electrostatic interaction. Generally, cobalt-nickel phosphate nano-ice creams $Co_3Ni_3(PO_4)_4$ NICs are synthesized via mild hydrothermal method and functionalized via polyethyleneimine (PEI). Then Au NPs are adsorbed on the surface of $Co_3Ni_3(PO_4)_4$ NIC via Au-N weak interaction to fabricate Au@$Co_3Ni_3(PO_4)_4$ NICs. Owing to the important roles of Au@$Co_3Ni_3(PO_4)_4$ in exhibiting excellent electrocatalytic activity,

* Corresponding author. Tel.: +86-23-68367392
E-mail address: liudf2009@swu.edu.cn

as well as preventing the deposition of negatively charged oxidation product induced electrode passivation, luminol in the nanohybrids (LH-Au@$Co_3Ni_3(PO_4)_4$) gives strong and stable ECL intensity in the neutral condition. Moreover, the ECL emission of luminol is obviously quenched based on the resonance energy transfer (RET) between luminol as donor and cytochrome c as accepter. Hence, a sensitive ECL biosensor is successfully fabricated for the quantitative determination of Cyt c in cell lysates and exhibits wide linear ranges of 1.0×10^{-4} – 0.5×10^{-5} and 0.5×10^{-5} – 1.0×10^{-8} M, as well as a low detection limit of 2.48 nM. This novel sensing strategy will broaden the application of transition metal (Co, Ni) phosphates in bioassay.

Keywords: functionalized cobalt-nickel phosphate, electrocatalytic activity, signal stabilization, neutral condition, cytochrome c, cell lysates

1. Introduction

Apoptosis, the programmed cell death, is closely associated with degenerative disorders (excessive apoptosis), autoimmune disorders and cancers (inadequate apoptosis)[1-2]. The intrinsic apoptotic progress can be monitored via detecting the release of cytochrome c (Cyt c) from mitochondrial[1, 3-5]. Therefore, quantitative determination of Cyt c in cell lysates plays role key for the diagnosis of early stage apoptotic cells. Many efficient methods containing fluorescence[6], surface enhanced raman scattering (SERS)[7], mass spectrometry[8], electrochemical[9] and chemiluminescence[10], are developed for the determination of Cyt c. However, these proposed methods possess the disadvantages of low sensitivity, complex test step,

expensive equipment. Electrochemiluminescence (ECL) has drawn great attention for Cyt c detection attributed to the merits of low background noise, high sensitivity, rapidness and easy controllability[11-14]. Owing to the strong emission, low cost, and low oxidation potential, luminol becomes the most widely applied ECL luminophor [15-17]. However, most of the ECL studies on luminol and its analogues have been limited to strong alkaline solution. Up to now, much effort has been made to improve the ECL emission of luminol in the neutral condition, such as using novel nanomaterial as coreaction accelerator, improving the load capacity of luminol, and searching a new coreaction [18-21]. It has always been annoying that neither individual luminol nor the functionalized luminol can maintain a strong and stable ECL signal under continuous scanning conditions. In addition, we find that the ECL stability of luminol significantly decreases with increasing applied potential, which may be attributed to the electrode passivation caused by electrochemically degraded of luminol under high applied potential. Interestingly, the electrode passivation problem can be resolved via functionalizing luminophor using nanomaterials [22].

Transition metal (Co, Ni) phosphates, emerging nanomaterials, have attracted tremendous interest in the areas of enzyme-free glucose sensors, energy storage and supercapacitors [23-26] due to their outstanding electrocatalytic activity and high stability. Obviously, it's a good choice utilizing transition metal phosphates to functionalize luminol. Nevertheless, the immobilization for the luminol on cobalt-nickel phosphate ($Co_3Ni_3(PO_4)_4$) nano-composites is a challenge. Gold nanoparticles functionalized cobalt-nickel phosphate (Au@$Co_3Ni_3(PO_4)_4$) provides possibility for the loading of

luminol. Herein, three-dimensional (3D) cobalt-nickel phosphate nano-ice creams provide larger surface for the immobilization of luminol and at the same time catalyze the oxidation of BNQDs (co-reactant) into intermediate (BNQDs-$NH^{+\bullet}$), thus leading to the enhancement of luminol-BNQDs system ECL emission. For another, $Co_3Ni_3(PO_4)_4$ nanomaterial with abundant of negatively charged prevents the deposition of oxidation products by electrostatic repulsion, which can effectively slow down electrode passivation[27]. Boron nitride quantum dots (BNQDs), zero-dimensional nanomaterial, have aroused widespread research interest due to unique surface properties such as the quantum confinement, edge effects, and defect centers[28-29]. Recently, BNQDs with unique structures or functional groups can serve as efficient coreactants with the analogous enhancement mechanism of small molecules[30-31]. For example, Wang et al. have reported that BNQDs with rich amino functional groups can be used as efficient coreactants for boosting ECL intensity of luminol[32].

In this work, Au@$Co_3Ni_3(PO_4)_4$ NICs is firstly prepared via a brief method. Interestingly, a stable and strong ECL emission can be obtained in the neutral condition using Au@$Co_3Ni_3(PO_4)_4$ NICs modified luminol as signal probe. Simultaneously, ECL signals of luminol decrease as various concentration of Cyt c is added into detection solution owing to the resonance energy transfer (RET) between luminol and Cyt c. On the basis of above facts, a sensitive, selective and label-free ECL biosensor has been fabricated for the detection of Cyt c. In this strategy, $Co_3Ni_3(PO_4)_4$ NICs is synthesized via mild hydrothermal method and functionalized

by PEI. Then Au NPs are adsorbed on the surface of $Co_3Ni_3(PO_4)_4$ NIC via electrostatic interaction. Finally, Au@$Co_3Ni_3(PO_4)_4$ NICs functionalized luminol (LH-Au@$Co_3Ni_3(PO_4)_4$ NICs) are prepared successfully through a facile Au-N Weak interaction (Scheme 1A). Moreover, this work would offer a new insight into the knowledge of Transition metal phosphates, which is beneficial for its further application.

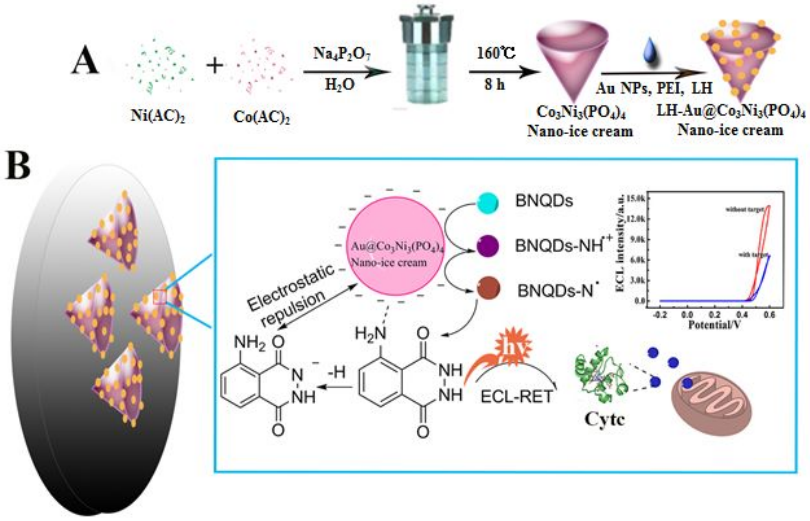

Scheme 1. (A) The illustration of synthetic process of LH-Au@$Co_3Ni_3(PO_4)_4$ composite. (B) The schematic representation of the stable and enhanced ECL emission of LH-Au@$Co_3Ni_3(PO_4)_4$ nanohybrid–coreactant system for Cyt c detection.

2. Experimental Section

2.1. Preparation of $Co_3Ni_3(PO_4)_4$ NICs

The $Co_3Ni_3(PO_4)_4$ NICs were synthesized through a facile hydrothermal method with some variations according to the literature reported previously [23]. Briefly, Nickel acetate (0.5 g), cobalt acetate (0.5 g), and sodium pyrophosphate (0.5 g) were dispersed in 10 mL of distilled water. Then the mixture stirred for 30 min and reacted

at 160 ˚C for 8 h. Finally, the product (yield is 79.7%) was washed by ultrapure water and ethanol three times and vacuum dried at 40 ˚C for 12 h.

2.2. Amino functionalization of $Co_3Ni_3(PO_4)_4$ NICs

The nanomaterial of NH_2-$Co_3Ni_3(PO_4)_4$ NICs was obtained according to previous literature with some modifications[33]. Generally, 200 mg prepared $Co_3Ni_3(PO_4)_4$ NICs were dispersed into 20 mL distilled water under ultrasonic, then 10 mL mixture solution with 0.6 M KCl and 2.5 mg·mL^{-1} PEI was added into above suspension under stirring. Subsequently, the mixture stirred vigorously at room temperature for a night, a homogeneous pink solution was achieved. Then, PEI could be adsorbed onto $Co_3Ni_3(PO_4)_4$ NICs via electrostatic attraction. Finally, the precipitates were centrifuged and washed three times to remove excessive KCl and PEI before it was redispersed in 10 mL of distilled water.

2.3. Construction of Au@$Co_3Ni_3(PO_4)_4$ NIC nanocomposite with different ratio

In this strategy, gold nanoparticles were prepared according to the previous study [34]. Au@$Co_3Ni_3(PO_4)_4$ NIC nanocomposites with different ratios were obtained by adding various volume of 20 mg·mL^{-1} NH_2-$Co_3Ni_3(PO_4)_4$ NIC into 10 mL above Au NPs colloid. The detailed experimental parameters were presented in Table S2. After addition of pink $Co_3Ni_3(PO_4)_4$ NICs, the color of mixture solution immediately changed from wine red into purple gray. Then the mixture stirred vigorously in room temperature for 6h. Finally, the products were centrifuged and washed three times and redispersed in 3 mL of distilled water. LH-Au@$Co_3Ni_3(PO_4)_4$ NIC was prepared via a simple method. Briefly, 1 mL 0.01 M luminol was added into 1 mL above purple gray

suspension, stirred vigorously at room temperature overnight. The precipitates were collected, washed several times and redispersed in 2 mL of ultrapure water for use. BNQDs were obtained through a facile bottom-up hydrothermal route [35].

2.4. Cell culture and apoptosis induction

Detailed procedure for the culture and apoptosis induction of embryonic kidney cells (HEK293T) is presented in the supplementary materials.

2.4. Preparation of modified electrodes.

First, a glassy carbon electrode (GCE, diameter 4 mm) was carefully polished with 0.05 μm Al_2O_3 powder, cleaned by brief ultrasonication with deionized water, ethanol (v:v = 1:1), nitric acid (v:v = 1:1) and distill water. For surface modification, the prepared LH-Au@$Co_3Ni_3(PO_4)_4$ NIC suspension was sonicated for 10 min. After that, 3 μL of above suspension was dropped onto the as-prepared GCE and dried in the air to be used as working electrode. Cyt c sensing measurements were performed by the MPI-E electrochemiluminescence analyzer in 2.5 mL 0.1 M PBS (pH 7.4) buffer containing 0.96 mg·mL^{-1} BNQDs.

3. Results and discussion

3.1. Characterization of nanomaterials

The $Co_3Ni_3(PO_4)_4$ were obtained through a facile hydrothermal method. As exhibited in Figure 1, the morphology of prepared nanomaterials was investigated via the scanning electron microscope (SEM). The SEM images in Figure S1A clearly show that $Co_3Ni_3(PO_4)_4$ exhibited an ice cream-like structure. Owing to the abundant negative charges at the surfaces, PEI is captured on the $Co_3Ni_3(PO_4)_4$ NIC via

electrostatic attraction (Figure S2a). At the same time, the zeta potential of nanomaterials changes from negative to positive (Figure S2b). The morphology of NH_2-$Co_3Ni_3(PO_4)_4$ has no change, and some small nanosheets are observed to be tightly wrapped around the nano-ice creams (Figure S1B,E). After modification of PEI, some spheres with an average size of 10 nm (Figure S1D) uniformly distribute on the surface of nanocomposite due to the electrostatic interaction and the covalent interaction of Au-N bond (Figure S1C,F). Moreover, the zeta potential of nanocomposite changes a lot (from 18.7 to 11.9 mV), further demonstrating the successful synthesis of Au@$Co_3Ni_3(PO_4)_4$ NIC (Figure S2d).

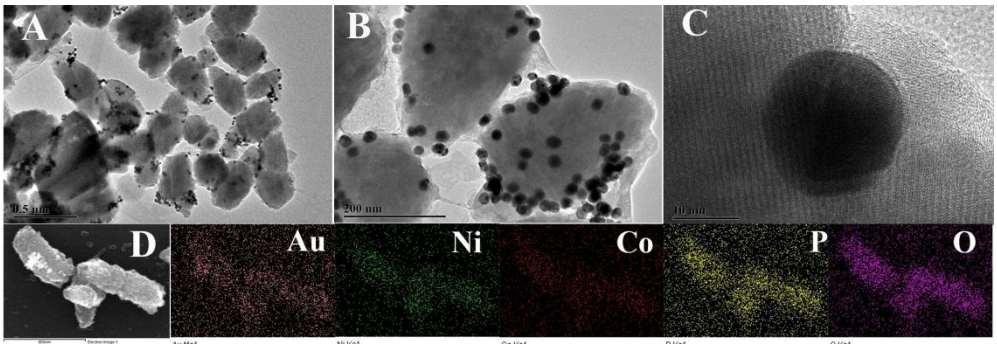

Figure 1. (A and B) TEM images of Au@$Co_3Ni_3(PO_4)_4$ with different magnification sizes. (C) HR-TEM image of gold nanoparticles. (D) Elemental mapping images of Au@$Co_3Ni_3(PO_4)_4$.

TEM images further reveal the three-dimensional (3D) morphology of Au@$Co_3Ni_3(PO_4)_4$ NIC. As shown in Figure 1A,B, ice cream-like structure with a length of 200-300 nm can be observed clearly. A large number of black dots corresponding to the Au NPs (Figure 1C) are adsorbed onto the surface of nano ice creams. No agglomeration of the Au NPs is observed, indicating that Au NPs are tightly anchored to the surface of $Co_3Ni_3(PO_4)_4$ NIC via Au-N bonds. Elemental

mapping demonstrates existence of Au, Co, Ni, P, and O elements and their homogeneous distribution within Au@$Co_3Ni_3(PO_4)_4$ NIC (Figure 1D).

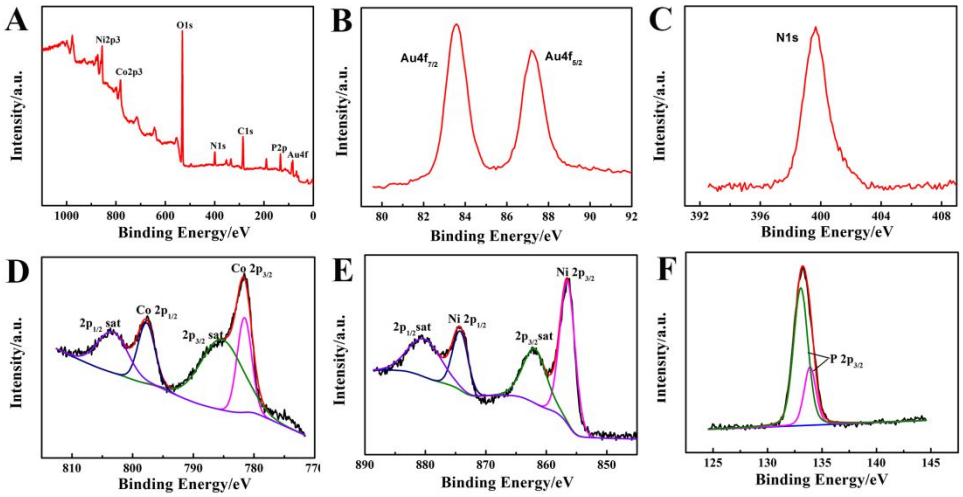

Figure 2. (A) XPS survey spectrum of Au@$Co_3Ni_3(PO_4)_4$ and narrow scan spectra of (B) Au 4f, (C) N 1s, (D) Co 2p, (E) Ni 2p and (F) P 2p, respectively.

To identify the valence state of elements above, XPS was carried out (Figure 2). According to the XPS analysis (Figure 2A−F), the peaks at 83.57 and 87.17 eV are assigned to $Au4f_{7/2}$ and $Au4f_{5/2}$, which is attributed to the spin–orbit splitting of doublet components[36-37]. The results are consistent with the previously reported literature, indicating the presence of Au^0 in the nanocomposites. A single peak at 399.67 in N1s spectrum is attributed to amide group, indicating successful amination of the $Co_3Ni_3(PO_4)_4$ NIC composite[38]. Co 2p spectrum can be deconvoluted into two peaks at around 781.59 and 797.72 eV corresponding to Co $2p_{3/2}$ and Co $2p_{1/2}$[23, 39]. Moreover, two strong shake-up satellite peaks located at 785.29 and 803.27eV are also observed, which verifies the surface enrichment of Co^{2+} ions [13, 39].Two major band energy peaks at 856.50 and 874.22 eV are ascribed to the Ni $2p_{3/2}$ and Ni $2p_{1/2}$ transitions. Similarly, two satellite peaks (861.90 and 880.10 eV) are also observed in

the spectrum of Ni 2p, indicating the presence of Ni (II) [23]. The peaks located at 133.05 and 133.90 eV are ascribed to the characteristic P $2p_{3/2}$ peaks of P (V) [23]. Results above further shows that prepared products are gold functionalized cobalt-nickel phosphate.

3.2. ECL and electrochemical characterization of nanomaterials

ECL behaviors of luminol and Au@$Co_3Ni_3(PO_4)_4$ functionalized luminol are investigated to explore the effect of nanocomposite. Compared with individual luminol, LH-Au@$Co_3Ni_3(PO_4)_4$ exhibits a brighter ECL emission (Figure 3A, curve a). The ECL enhancement phenomenon can be attributed to the large surface of 3D cobalt-nickel phosphate nano-ice creams, which can adsorb abundant Au NPs and give more attachment sites for luminol (Figure S1C,F). Additionally, electrochemical characterization was performed to explore the role of $Co_3Ni_3(PO_4)_4$ NIC. As shown in the Figure 3D, LH-Au@$Co_3Ni_3(PO_4)_4$ gives an more obvious oxidation peak, indicating that composite may have a great catalytic effect on the oxidation of BNQDs (co-reactant) and give rise more radical intermediate (BNQDs-$NH^{+\bullet}$). It should be noted that Au@$Co_3Ni_3(PO_4)_4$ not only enhance the ECL emission but also play a role key in the stabilization of the signal. The ECL signals of individual luminol and Au@$Co_3Ni_3(PO_4)_4$ functionalized luminol are recorded at a potential range -0.2 - 0.6V (Figure 3B,E). In the absence of Au@$Co_3Ni_3(PO_4)_4$, the ECL emission gradually decays under continuous potential scans, which may be ascribed to electrode passivation resulting from accumulation of oxidation product (L^-). Simultaneously, the oxidation rate of luminol accelerates with increasing of the

applied potential and negatively charged products rapidly cover the electrode surface to hamper further electron transfer at the electrode [27]. Thus, after increasing the voltage to 0.8V, the ECL intensity start to rapidly degrade and keep a lower signal (Figure 3C,F). Herein, Au@$Co_3Ni_3(PO_4)_4$ composites with abundant of negatively charged (Figure S2) prevent the deposition of oxidation product through electrostatic repulsion. After functionalizing the nanocomposite, the LH-Au@$Co_3Ni_3(PO_4)_4$ NICs give more stable and strong signal compared with individual luminol.

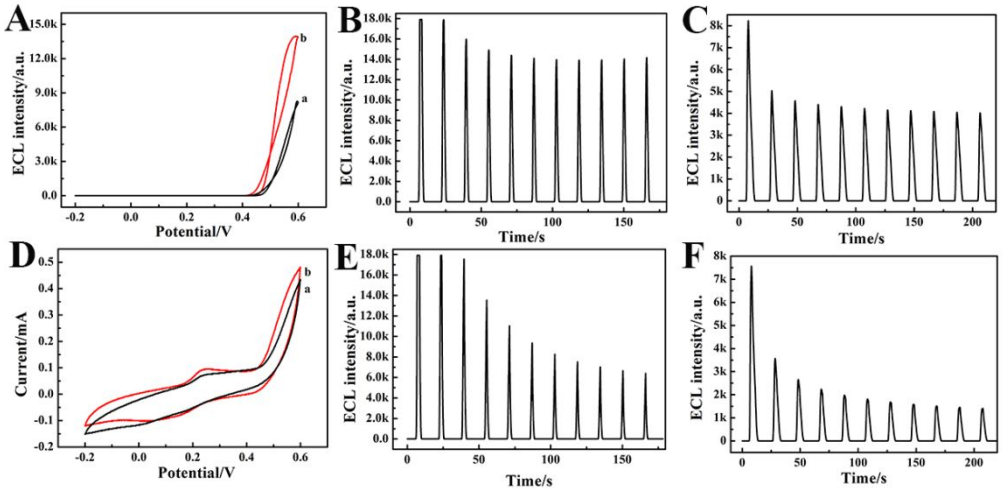

Figure 3. (A) ECL behaviors of LH (a) and LH-Au@$Co_3Ni_3(PO_4)_4$ (b) in 0.1 M PBS (pH = 7.4) containing 0.96 mg·mL^{-1} BNQDs. (D) Corresponding CV curves. ECL emission from individual LH-Au@$Co_3Ni_3(PO_4)_4$ (B, C) and LH (E, F) under continuous cyclic scans for 11 cycles with different potential window: (B and E) -0.2 to 0.6 V; (C and F) -0.2 to 0.8 V in 0.1 M PBS (pH 7.4). Scan rate: 100 mV·s^{-1}.

3.3. Detection principle of Cyt c

To explore the detection principle of Cyt c in the ECL system, the ECL and spectral behaviors were investigated in the presence of coreactant. As shown in the Figure 4A, LH-Au@$Co_3Ni_3(PO_4)_4$ exhibits a strong ECL emission (about 14000 a.u.).

In the presence of Cyt c, ECL intensity of nanocomposite obviously decreases (about 6500a.u.), indicating that Cyt c could inhibit ECL signal of luminol. To confirm if there is resonance energy transfer between Cyt c and luminol, the UV-vis spectrum of Cyt c and fluorescence spectroscopy of luminol were collected under the excitation of 393 nm. As seen, Cyt c gives an absorption maximum at 408 nm, whereas luminol exhibits a fluorescence emission at 427 nm. Clearly, there is a significant spectral overlap, indicating the resonance energy transfer between Cyt c and luminol (Figure 4B). It is based on this resonance energy transfer that the ECL emission of luminol is significantly weakened. The schematic principle of the ECL inhibition method for Cyt c detection is shown in Scheme 1B.

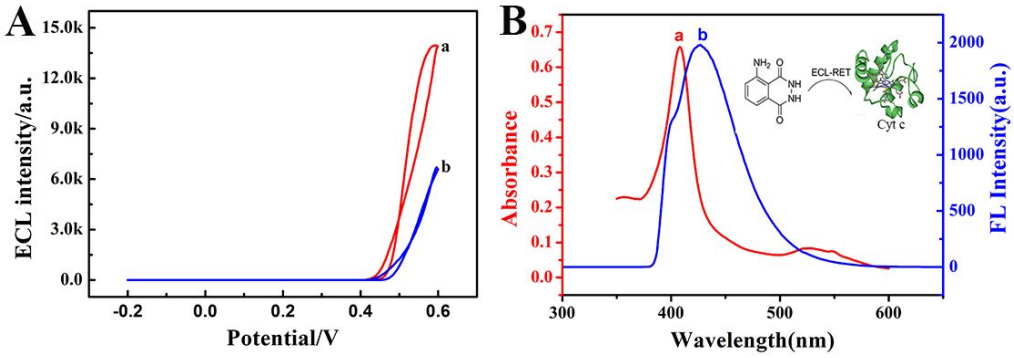

Figure 4. (A) ECL spectra of LH-Au@$Co_3Ni_3(PO_4)_4$ in the absence (a) and presence (b) of 0.1 mM Cyt c in 0.1 M PBS solution (pH 7.4). (B) The UV-vis absorption spectrum of Cyt c (a) and the fluorescence emission spectrum of the luminol (b). Scan rate: 100 $mV \cdot s^{-1}$.

3.4. Optimization of experimental parameters

To obtain an excellent property nanomaterial, the ratios of Co and Ni in the nanomaterial and the concentration of the $Co_3Ni_3(PO_4)_4$ were investigated in this work (Figure S3A,B). The cobalt-nickel phosphate nano-ice creams with different

ratios were synthesized through a facile hydrothermal method (the detailed experimental parameters are listed in Table S1). As seen, the Sample 3 exhibits (Co:Ni = 5:5) maximum ECL response in pH = 7.4 PBS containing 0.01 M luminol, indicating 5:5 is the optimal ratio. Owing to the immobilization problem of the luminol on cobalt-nickel phosphate nanocomposite, Au NPs are selected as connecting element. Thus, the concentrations of cobalt-nickel phosphate in the Au@$Co_3Ni_3(PO_4)_4$ nanocomposite are vital factor. Here, Au@$Co_3Ni_3(PO_4)_4$ NIC nanocomposites with different ratios are obtained by adding various volume (0.5 - 2.5 mL) of $Co_3Ni_3(PO_4)_4$ (Co:Ni = 5:5) into same volume of Au NPs colloid and the ECL emission achieved a maximum value at 2.0 mL(about 2.86 $mg \cdot mL^{-1}$). Thus, 2.86 $mg \cdot mL^{-1}$ is the optimum concentration of $Co_3Ni_3(PO_4)_4$ (Co:Ni = 5:5).

After optimizing nanomaterial property, some important influencing parameters about ECL biosensor are also evaluated. The concentration of BNQDs is a crucial factor for the ECL system. As shown in the Figure S3C, the ECL emission achieves the maximum value at 1.00 $mg \cdot mL^{-1}$. Thus, 1.00 $mg \cdot mL^{-1}$ is selected as the optimum concentration of BNQDs in Cyt c detection experiments. The modified volume of LH-Au@$Co_3Ni_3(PO_4)_4$ is also an important factor for the ECL emission. Hence, the effect of modified volume is optimized in the range of 1 – 6 μL (Figure S3D). The ECL intensity gradually increases as the volume increased and achieved plateau at 3 μL. So 3 μL of LH-Au@$Co_3Ni_3(PO_4)_4$ is used for the following experiments.

3.5 Detection of Cyt c with ECL biosensor

The concentration-dependent ECL biosensor performance is evaluated in optimal

condition. Herein, I and I_0 are chosen as the ECL intensity of in presence and absence of Cyt c, and $(I_0 - I) / I_0$ is the ECL inhibition efficiency. As shown in Figure 5A, the ECL emission decreases gradually with increasing concentration of Cyt c. Simultaneously, A good linear relationship is obtained between the ECL inhibition efficiency and the logarithm of concentration of Cyt c in the ranges of $1.0 \times 10^{-4} – 0.5 \times 10^{-5}$ M and $0.5 \times 10^{-5} – 1.0 \times 10^{-8}$ M (Figure 5B). The homologous linear equation are $(I_0 - I) / I_0 = 1.262 + 0.187\lg c$ ($R^2 = 0.9924$) and $(I_0 - I) / I_0 = 0.780 + 0.993\lg c$ ($R^2 = 0.9920$), and the limit of detection is 2.48 nM (S/N = 3). It can be seen that the fabricated biosensor has much wider detection compared with previous works (Table S3), suggesting a great potential for quantitative determination of Cyt c using the biosensor.

3.6 Stability and Selectivity of the ECL biosensor

Excellent stability is a key indicator for the assessment of biosensor performance. As illustrated in Figure 5C, the ECL emission is observed under nine cycles of successive pulse potential. It is obvious that a relative stable ECL emission has been achieved with the relative standard deviation (RSD) of 2.46 %, indicating the proposed biosensor has a good stability in Cyt c detection. To further evaluate the selectivity of the constructed ECL sensor, bovine serum albumin (BSA, 1 $mg \cdot mL^{-1}$), glutathione (GSH, 1.0 mM), ascorbic acid (AA, 1.0 mM), glucose (1.0 mM), hemin (1.0 mM) and $FeCl_3$ (1.0 mM) are selected as possible interferences (Figure 5D). It can be seen that 0.1 mM Cyt c could trigger significant inhibition of ECL intensity. However, interference substances with high concentration (about 10 times higher than

the concentration of Cyt c) have a little inhibition effects. Therefore, prepared ECL platform has excellent selectivity toward the Cyt c.

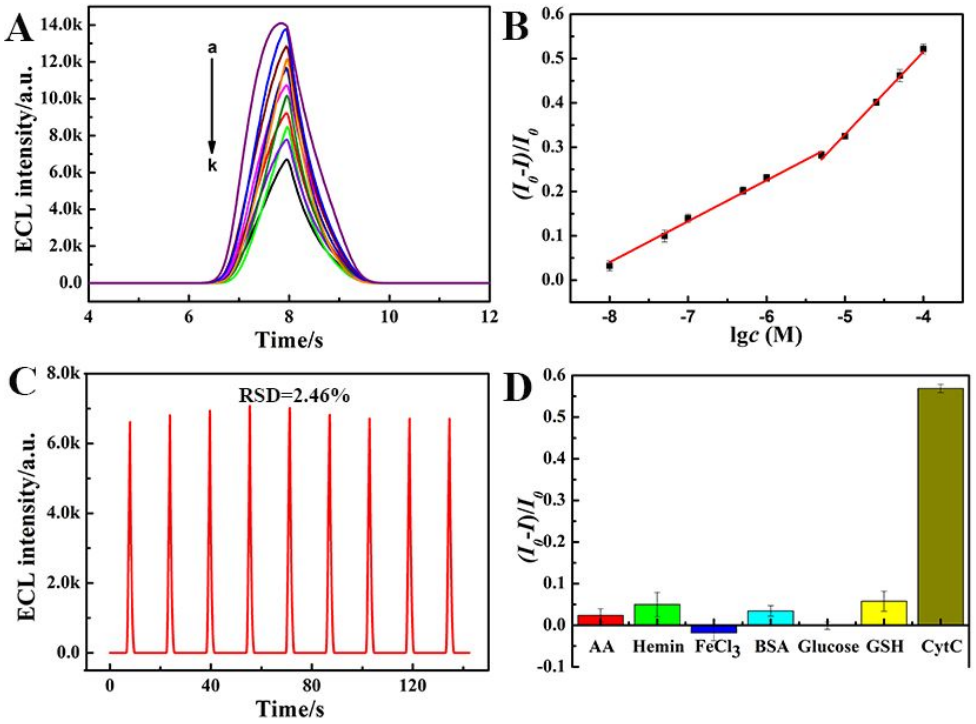

Figure 5. (A) ECL-time curves of constructed sensor with different Cyt c concentrations (M): (a) 0, (b) 1.00×10^{-8}, (c) 0.50×10^{-7}, (d) 1.00×10^{-7}, (e) 0.50×10^{-6}, (f) 1.00×10^{-6}, (g) 0.50×10^{-5}, (h) 1.00×10^{-5}, (i) 0.25×10^{-4}, (j) 0.50×10^{-4} and (k) 1.00×10^{-4}. (B) Calibration curves of ECL biosensor. (C) The stability of the prepared ECL platform under continuous cyclic scans for nine cycles with 0.1 mM Cyt c. (D) The selectivity of proposed ECL sensor: AA (1.0 mM), Hemin (1.0 mM), $FeCl_3$ (1.0 mM), BSA (1.0 mg·mL^{-1}), Glucose (1.0 mM), GSH (1.0 mM) and Cyt c (0.1 mM)

3.7 Analysis of Released Cyt c during apoptosis

Considering the good stability and selectivity of the constructed ECL biosensor, we detect the released Cyt c via standard addition method using this analytical

platform (Table 1). In this work, human embryonic kidney cells HEK293T are selected to study the early stage of apoptosis. 25 μL 2 × 10^6 cell mL^{-1} apoptosis supernatant is diluted to 2.5 mL PBS (pH = 7.4) and a certain amount Cyt c (0.5 - 1.4 μM) is spiked into above sample. Concentration of Cyt c is 0.04 μM detected with proposed biosensor in apoptosis supernatant sample (consistent with the standard method in the reference[2]). Moreover, the recovery ranges from 100.10 to 102.22 % and the precision for three replicate detections of Cyt c is also in a satisfactory range of 0.53 − 2.52 %, indicating the feasibility and reliability of the proposed method Cyt c detection in real samples.

Table 1 Cyt c detection in HEK293T cells and spiked samples (n = 3) treated with RIPA buffer

Sample number	Spiked (μM)	Found (μM)	Recovery (%, n=3)	RSD (%, n=3)
1	0	0.04	-	1.13
2	0.50	0.55	102.22	0.92
3	0.90	0.95	101.30	0.53
4	1.40	1.45	100.10	2.52

4. Conclusion

A novel ECL biosensor was constructed based on gold functionalized cobalt-nickel phosphate 3D nano-ice cream employed as carrier of luminol for the Cyt c detection in cell lysates. Herein, cobalt-nickel phosphate 3D nano-ice creams provide larger surface for the immobilization of luminol and at the same time catalyze the oxidation of BNQDs (co-reactant) and luminol (luminopher), leading to the enhancement of luminol-BNQDs system ECL emission. Moreover, $Co_3Ni_3(PO_4)_4$

nanomaterial with abundant of negatively charged prevents the deposition of oxidation products by electrostatic repulsion, effectively slowing down electrode passivation and realizing stabilization of ECL intensity. Therefore, LH-Au@$Co_3Ni_3(PO_4)_4$ composite exhibited strong and stable ECL activity compared with individual luminol in neutral condition. Simultaneously, ECL signal of luminol decreased as various concentration of Cyt c was added into detection solution owing to the resonance energy transfer (RET) between luminol and Cyt c. The proposed ECL sensing platform showed a sensitive and selective response to Cyt c, which was important for early stage detection of apoptosis. Moreover, this work would offer a new insight into the knowledge of Transition metal phosphates, which was beneficial for its further application.

Supporting Information

Reagents and chemicals; Instrument; Cell culture and apoptosis induction; The SEM images and Zeta potential of $Co_3Ni_3(PO_4)_4$, NH_2-$Co_3Ni_3(PO_4)_4$, Au NPs and Au@$Co_3Ni_3(PO_4)_4$; Optimization of experimental conditions; ECL behavior of individual BNQDs; ECL signals of LH-Au@$Co_3Ni_3(PO_4)_4$ in PBS buffer with different pH and ECL intensity of LH-Au@$Co_3Ni_3(PO_4)_4$ with and without BNQDs; The calculation procedure of the LOD; Experimental parameters for the synthesis of $Co_3Ni_3(PO_4)_4$ and Au@$Co_3Ni_3(PO_4)_4$ nanocomposite; Comparison with other strategies in Cyt c detection.

Acknowledgments

We sincerely acknowledge the financial support of the National Natural Science

Foundation of China (No. 61503309) and the Fundamental Research Funds for the Central Universities (XDJK2015C019) and the Dr. Start-up Foundation of the Southwest University (SWU113074).

References

(1) Chen, T. T.; Tian, X.; Liu, C. L.; Ge, J.; Chu, X.; Li, Y. Fluorescence Activation Imaging of Cytochrome c Released from Mitochondria Using Aptameric Nanosensor. *J. Am. Chem. Soc.* **2015,** *137*, 982-989.

(2) Shamsipur, M.; Molaabasi, F.; Hosseinkhani, S.; Rahmati, F. Detection of Early Stage Apoptotic Cells Based on Label-Free Cytochrome c Assay Using Bioconjugated Metal Nanoclusters as Fluorescent Probes. *Anal. Chem.* **2016,** *88*, 2188-2197.

(3) Waterhouse, N. J.; Trapani, J. A. A New Quantitative Assay for Cytochrome c Release in Apoptotic cells. *Cell. Death. Differ.* **2003,** *10*, 853-855.

(4) Zhang, S.; Zhu, S.; Yang, L.; Zheng, Y.; Gao, M.; Wang, S.; Zeng, J. Z.; Yan, X. High-Throughput Multiparameter Analysis of Individual Mitochondria. *Anal. Chem.* **2012,** *84*, 6421-6428.

(5) Song, J. M.; Kasili, P. M.; Griffin, G. D.; Vo-Dinh, T. Detection of Cytochrome c in a Single Cell Using an Optical Nanobiosensor. *Anal. Chem.* **2004,** *76*, 2591-2594.

(6) Amin, R. M.; Elfeky, S. A.; Verwanger, T.; Krammer, B. Fluorescence-Based CdTe Nanosensor for Sensitive Detection of Cytochrome c. *Biosens. Bioelectron.* **2017,** *98*, 415-420.

(7) Xia, Y.; Gao, P.; Qiu, X.; Xu, Q.; Gan, S.; Yang, H.; Huang, S. Aptasensor Based

on Triplex Switch for SERS Detection of Cytochrome c. *Analyst* **2012,** *137*, 5705-5709.

(8) Liu, J. M.; Yan, X. P. Ultrasensitive, Selective and Simultaneous Detection of Cytochrome c and Insulin Based on Immunoassay and Aptamer-Based Bioassay in Combination with Au/Ag Nanoparticle Tagging and ICP-MS Detection. *J. Anal. At. Spectrom.* **2011,** *26*, 1191-1197.

(9) Wen, Q.; Zhang, X.; Cai, J.; Yang, P. H. A Novel Strategy for Real-Time and In Situ Detection of Cytochrome c and Caspase-9 in Hela Cells During Apoptosis. *Analyst* **2014,** *139*, 2499-2506.

(10) Li, X.; Liu, H.; He, X.; Song, Z. Determination of Cytochrome c in Human Serum and Pharmaceutical Injections Using Flow Injection Chemiluminescence. *Appl. Microbiol. Biotechnol.* **2010,** *160*, 1065-1073.

(11) Jiang, X.; Wang, H.; Zhuo, Y.; Yuan, R.; Chai, Y. Electrochemiluminescence Biosensor Based on 3-D DNA Nanomachine Signal Probe Powered by Protein-Aptamer Binding Complex for Ultrasensitive Mucin 1 Detection. *Anal. Chem.* **2017,** *89*, 4280-4286.

(12) Dong, Y. P.; Gao, T. T.; Zhou, Y.; Zhu, J. J. Electrogenerated Chemiluminescence Resonance Energy Transfer between Luminol and CdSe@ZnS Quantum Dots and Its Sensing Application in the Determination of Thrombin. *Anal. Chem.* **2014,** *86*, 11373-11379.

(13) Wang, S.; Zhao, Y.; Wang, M.; Li, H.; Saqib, M.; Ge, C.; Zhang, X.; Jin, Y. Enhancing Luminol Electrochemiluminescence by Combined Use of Cobalt-Based

Metal Organic Frameworks and Silver Nanoparticles and Its Application in Ultrasensitive Detection of Cardiac Troponin I. *Anal. Chem.* **2019,** *91*, 3048-3054.

(14) Li, M.; Wang, C.; Chen, L.; Liu, D. A Novel Electrochemiluminescence Sensor Based on Resonance Energy Transfer System between Nitrogen Doped Graphene Quantum Dots and Boron Nitride Quantum Dots for Sensitive Detection of Folic Acid. *Anal. Chim. Acta.* **2019,** *1090*, 57-63.

(15) Wu, L.; Ding, F.; Yin, W.; Ma, J.; Wang, B.; Nie, A.; Han, H. From Electrochemistry to Electroluminescence: Development and Application in a Ratiometric Aptasensor for Aflatoxin B1. *Anal. Chem.* **2017,** *89*, 7578-7585.

(16) Kitte, S. A.; Gao, W.; Zholudov, Y. T.; Qi, L.; Nsabimana, A.; Liu, Z.; Xu, G. Stainless Steel Electrode for Sensitive Luminol Electrochemiluminescent Detection of H_2O_2, Glucose, and Glucose Oxidase Activity. *Anal. Chem.* **2017,** *89*, 9864-9869.

(17) Zhang, M.; Yuan, R.; Chai, Y.; Chen, S.; Zhong, H.; Wang, C.; Cheng, Y. A Biosensor for Cholesterol Based on Gold Nanoparticles-Catalyzed Luminol Electrogenerated Chemiluminescence. *Biosens. Bioelectron.* **2012,** *32*, 288-292.

(18) Liu, W.; Chen, A.; Li, S.; Peng, K.; Chai, Y.; Yuan, R. Perylene Derivative/Luminol Nanocomposite as a Strong Electrochemiluminescence Emitter for Construction of an Ultrasensitive MicroRNA Biosensor. *Anal. Chem.* **2019,** *91*, 1516-1523.

(19) Wang, C.; Chen, L.; Wang, P.; Li, M.; Liu, D. A Novel Ultrasensitive Electrochemiluminescence Biosensor for Glutathione Detection Based on Poly-L-lysine as Co-reactant and Graphene-Based Poly(luminol/aniline) as

Nanoprobes. *Biosens. Bioelectron,* **2019,** *133*, 154-159.

(20) Wu, F. F.; Zhou, Y.; Zhang, H.; Yuan, R.; Chai, Y. Q. Electrochemiluminescence Peptide-Based Biosensor with Hetero-Nanostructures as Coreaction Accelerator for the Ultrasensitive Determination of Tryptase. *Anal. Chem.* **2018,** *90*, 2263-2270.

(21) Zhang, H.; Han, Z.; Wang, X.; Li, F.; Cui, H.; Yang, D.; Bian, Z. Sensitive Immunosensor for N-terminal Pro-brain Natriuretic Peptide Based on N-(aminobutyl)-N-(ethylisoluminol)-Functionalized Gold Nanodots/Multiwalled Carbon Nanotube Electrochemiluminescence Nanointerface. *ACS Appl. Mater. interfaces* **2015,** *7*, 7599-7604.

(22) Chen, L.; Zeng, X.; Si, P.; Chen, Y.; Chi, Y.; Kim, D. H.; Chen, G. Gold Nanoparticle-Graphite-Like C_3N_4 Nanosheet Nanohybrids Used for Electrochemiluminescent Immunosensor. *Anal. Chem.* **2014,** *86*, 4188-4195.

(23) Shu, Y.; Li, B.; Chen, J.; Xu, Q.; Pang, H.; Hu, X. Facile Synthesis of Ultrathin Nickel-Cobalt Phosphate 2D Nanosheets with Enhanced Electrocatalytic Activity for Glucose Oxidation. *ACS Appl. Mater. interfaces* **2018,** *10*, 2360-2367.

(24) Minakshi, M.; Mitchell, D.; Jones, R.; Alenazey, F.; Watcharatharapong, T.; Chakraborty, S.; Ahuja, R. Synthesis, Structural and Electrochemical Properties of Sodium Nickel Phosphate for Energy Storage Devices. *Nanoscale* **2016,** *8*, 11291-11305.

(25) Pang, H.; Liu, Y.; Li, J.; Ma, Y.; Li, G.; Ai, Y.; Chen, J.; Zhang, J.; Zheng, H. Cobalt Phosphite Microarchitectures Assembled by Ultralong Nanoribbons and Their

Application as Effective Electrochemical Capacitor Electrode Materials. *Nanoscale* **2013,** *5*, 503-507.

(26) Kim, H.; Park, J.; Park, I.; Jin, K.; Jerng, S. E.; Kim, S. H.; Nam, K. T.; Kang, K. Coordination Tuning of Cobalt Phosphates Towards Efficient Water Oxidation Catalyst. *Nat. Commun.* **2015,** *6*, No. 8253

(27) Ye, R.; Huang, L.; Qiu, B.; Song, Z.; Lin, Z.; Chen, G. Cathodic Electrochemiluminescent Behavior of Luminol at Nafion-Nano-TiO_2 Modified Glassy Carbon Electrode. *Luminescence* **2011,** *26*, 531-535.

(28) Lin, L.; Xu, Y.; Zhang, S.; Ross, I. M.; Ong, A. C. M.; Allwood, D. A. Fabrication and Luminescence of Monolayered Boron Nitride Quantum Dots. *Small* **2014,** *10*, 60-65.

(29) Li, H.; Tay, R. Y.; Tsang, S. H.; Zhen, X.; Teo, E. H. T. Controllable Synthesis of Highly Luminescent Boron Nitride Quantum Dots. *Small* **2015,** *11*, 6491-6499.

(30) Xing, H.; Zhai, Q.; Zhang, X.; Li, J.; Wang, E. Boron Nitride Quantum Dots as Efficient Coreactant for Enhanced Electrochemiluminescence of Ruthenium(II) Tris(2,2′-bipyridyl). *Anal. Chem.* **2018,** *90*, 2141-2147.

(31) Zhang, Y.; Chai, Y.; Wang, H.; Yuan, R. Target-Induced 3D DNA Network Structure as a Novel Signal Amplifier for Ultrasensitive Electrochemiluminescence Detection of MicroRNAs. *Anal. Chem.* **2019,** *91*, 14368-14374.

(32) Wang, C.; Li, M.; Wang, P.; Liu, D. An Electrochemiluminescence Biosensor Based on Boron Nitride Quantum Dots as Novel Coreactant for Quantitative Determination of Concanavalin A. *Microchim. Acta.* **2020,** *187*, No. 409.

(33) Zhu, X.; Zhai, Q.; Gu, W.; Li, J.; Wang, E. High-Sensitivity Electrochemiluminescence Probe with Molybdenum Carbides as Nanocarriers for alpha-Fetoprotein Sensing. *Anal. Chem.* **2017,** *89*, 12108-12114.

(34) Frens, G. Controlled Nucleation for Regulation of Particle-Size in Monodisperse Gold Suspensions. *Nat. Phy. Sci.* **1973,** *241*, 20-22.

(35) Xing, H.; Zhai, Q.; Zhang, X.; Li, J.; Wang, E. Boron Nitride Quantum Dots as Efficient Coreactant for Enhanced Electrochemiluminescence of Ruthenium(II) Tris(2,2'-bipyridyl). *Anal. Chem.* **2018,** *90*, 2141-2147.

(36) Cui, H.; Wang, W.; Duan, C. F.; Dong, Y. P.; Guo, J. Z. Synthesis, Characterization, and Electrochemiluminescence of Luminol-Reduced Gold Nanoparticles and Their Application in a Hydrogen Peroxide Sensor. *Chemistry* **2007,** *13*, 6975-6984.

(37) Lengke, M. F.; Fleet, M. E.; Southam, G. Morphology of Gold Nanoparticles Synthesized by Filamentous Cyanobacteria from Gold(I)-Thiosulfate and Gold(III)-Chloride Complexes. *Langmuir* **2006,** *22*, 2780-2787.

(38) Puniredd, S. R.; Srinivasan, M. P. Covalent Molecular Assembly in Supercritical Carbon Dioxide: A Comparative Study between Amine- and Anhydride-Derivatized Surfaces. *Langmuir* **2006,** *22*, 4092-4099.

(39) Zhang, J.; Yang, Y.; Zhang, Z.; Xu, X.; Wang, X. Rapid Synthesis of Mesoporous $Ni_xCo_{3-x}(PO_4)_2$ Hollow Shells Showing Enhanced Electrocatalytic and Supercapacitor Performance. *J. Mater. Chem. A.* **2014,** *2*, 20182-20188.

Table of Contents (TOC) graphic